High-density properties of integral-equation theories of fluids: Universal analytic structure and details for the one-component plasma

Yaakov Rosenfeld
Nuclear Research Centre—Negev, P.O. Box 9001, 84190 Beer-Sheva, Israel
(Received 11 October 1985)

We study the analytic properties of the hypernetted-chain (HNC) and soft-mean-spherical (SMSA) theories in the asymptotic high-density limit (AHDL). The scaling properties of the inverse power potentials lead to the introduction of the SMSA-Ewald functions, which correspond to the "overlap-volume" functions for hard spheres. The HNC and SMSA theories for soft interactions, as well as the Percus-Yevick theory for hard spheres, feature the same AHDL analytic structure of the pair correlation functions, which is dictated by the hard-sphere Ewald functions. The general discussion is supplemented by detailed results for the one-component plasma. Implications to the analysis of the density-functional theory, of dense matter, near its exact Thomas-Fermi limit are pointed out.

I. INTRODUCTION

Integral-equation theories of fluids have been the object of extensive studies in recent decades, and have found many applications for quite disparate kinds of physical systems.[1] In most applications these equations must be solved numerically and the solution becomes increasingly more difficult as the density (or the reduced coupling constant for the strength of the interaction) increases. It is hardly surprising, therefore, that the few cases that could be solved analytically attracted relatively high attention, i.e., (i) the solution of the Percus-Yevick equation for hard spheres[2] (PYHS) played an important role in the development and application of modern perturbation theory for liquids;[1,3] (ii) the solution of the mean spherical approximation (MSA) for the primitive model of electrolytes,[4] and its generalization for centrally charged, arbitrary hard-sphere mixtures,[5] still play an important role in the study of molten salts and electrolytes;[1,6] (iii) the modification of the MSA to treat soft interactions[7,8] (SMSA) found applications for plasmas[9] and colloidal dispersions;[10] (iv) the solution of the MSA with Yukawa closure[11] found applications as a parametric fit for simulation data.[12] This list can be carried on and on. It should be noted, however, that these analytic solutions still involve parametric nonlinear algebraic equations for various coefficients, and these can be solved only numerically. Partly due to this complexity, especially for mixtures, there has not emerged from these solutions a general picture regarding their analytic form, its dependence on the dimensionality D, and its possible physical meaning, as related to the pair potential $\phi(r)$.

Starting from the analysis of the universality of the bridge functions,[13] it has become increasingly clear that a proper fundamental approach to the study and application of integral equations (especially those obtained from the diagrammatic analysis of the pair functions) must be done using the modified hypernetted-chain (MHNC) scheme.[14] In this scheme, the hypernetted-chain (HNC) equation is solved for a modified potential (that includes the contribution of the bridge functions) which corresponds to the physical pair potential in the HNC special case. The HNC equation has not been solved analytically for any physically interesting potential, and the analysis of the HNC and MHNC has to rely on the numerical solutions.

Much work on the HNC and SMSA theories was done in recent years in connection with the one-component plasma[15] (OCP), especially regarding density-functional theories of ionized matter,[16] and as models for liquid metals.[17] The OCP provides a reference in a perturbative treatment of such systems. The similarity between the HNC and SMSA results for the OCP prompted a detailed study of the thermodynamics of these theories as related to their closure relations for the pair functions.[18] It was found that both theories share many common features, especially regarding their variational free-energy functional of the pair functions. It thus seemed that the SMSA, with its available analytic solution, can provide a starting point for the analysis of the HNC theory for soft (without hard-core) potentials. The analytic form of the PYHS equation of state (EOS), the corresponding success of Y expansion[19] and scaled particle theories for hard particles,[20] and the simple and accurate asymptotic high-density forms for the OCP EOS,[21] suggested the study of the asymptotic high-density limit (AHDL) of these theories.[22]

A novel approach to the analysis of the AHDL properties of the HNC and SMSA theories was proposed,[23] by which it was possible to establish a large body of interesting new results, valid for arbitrary D and for mixtures. (i) The HNC and SMSA integral-equation theories for soft potentials, together with the variational perturbation theory (based on the PYHS as a reference), are all identical in the AHDL; they share the same Madelung energy that constitutes an exact lower bound to the true potential energy of the system. (ii) This lower-bound Madelung energy can be evaluated either by solving a boundary-value problem or by employing the PYHS pair functions. (iii)

In the AHDL these theories feature the generally unphysical property of a space-filling-excluded volume region [namely, $g(r<2a_{WS})=0$, where WS denotes Wigner-Seitz] corresponding to total packing fraction equal to unity. (iv) A well-defined physical meaning for the direct correlation functions (DCF's) has been found for both hard-core interactions (as overlap volumes) and soft interactions (as interaction between "smeared particles"). (v) The general analytic solution of the MSA for any Green's-function potential and for hard spheres was obtained, and (vi) its relation to the Onsager procedure[24] for obtaining exact lower bounds for the energy was established.

Ideas generated through the study of the AHDL problem have already been useful for the study of (i) the EOS of plasma mixtures,[25] (ii) the isotropic-nematic transition of line charges,[26] and (iii) the coupling of micellar growth to the degree of alignment.[27] (iv) Study of the AHDL problem also led to the introduction of a new and general approach to the statistical thermodynamics of complex systems (e.g., water, colloidal dispersions, polyelectrolytes, micelles, etc.) modeled as hard objects with embedded charge distributions.[28]

In this paper we continue our study of the AHDL properties of theories for fluids, with the aim of further clarifying the connection between the variational boundary-value problem and the analytic form of the pair correlation functions (PCF's). Some points regarding the PYHS and MSA are considered, but the main body of the paper concerns the analytic structure of the SMSA and HNC theories for soft interactions near the AHDL. In particular, detailed SMSA and HNC results for the OCP are compared. The paper is structured as follows.

Section II contains a short review of the HNC and SMSA theories. In Sec. III the general SMSA variational boundary-value problem is formulated and general results for Green's-function potentials are presented. The special scaling properties of the inverse power potentials as borne out by the variational problem are featured, the AHDL-SMSA Ewald functions are introduced, and their properties are discussed. The general analytic form of the SMSA pair correlation functions in the AHDL is analyzed in Sec. IV, and the corresponding expressions for the Madelung energy are presented. The AHDL properties of the HNC theory are examined in Sec. V. We find that, in addition to the mapping of the AHDL-HNC on the AHDL-SMSA variational problem, the general analytic structure of the HNC pair correlation function near the AHDL is very similar to that of the SMSA. Section VI is devoted to a detailed comparison of the HNC and SMSA theories for the OCP, with special emphasis on the analytic structure. Section VII is devoted to a brief summary of our results and some of their implications. We discuss, in particular, the density-functional theory[16] for dense plasmas near its exact Thomas-Fermi high-density limit. In Appendix A we display the connection between the PYHS Ewald function and the Laplace transform of the AHDL pair correlation function, whose residues are calculated in Appendix B. To make the paper more self-contained, we quote, in Appendix C, the main results of Palmer and Weeks[29] for charged hard spheres.

II. A BRIEF REVIEW OF THE HNC AND SMSA THEORIES

The HNC and SMSA integral equations are obtained from the Ornstein-Zernike (OZ) relation between the direct correlation function (DCF) $c(r)$ and the pair correlation function (PCF) $g(r)=h(r)+1$,

$$h(r)=c(r)+\rho\int h(|\mathbf{r}-\mathbf{r}'|)c(|\mathbf{r}'|)d\mathbf{r}' , \tag{1}$$

and the "closure" relations

$$c(r)+\beta\phi(r)=g(r)-1-\ln g(r)\geq 0 \tag{2}$$

for the HNC, and

$$g(r)=0, \quad r<R; \quad c(r)+\beta\phi(r)=0, \quad r>R \tag{3a}$$

for the MSA, while

$$g(r=R+0)=0 \tag{3b}$$

is the SMSA condition. $\rho=N/V$ is the number density, $\beta=(k_BT)^{-1}$ the inverse temperature, $\phi(r)$ the pair potential, and R the MSA hard-core diameter. The MSA equation for hard spheres, i.e., with $c(r>R)=0$, is identical to the Percus-Yevick equation for hard spheres (PYHS).

Three alternative routes for obtaining the equation of state (EOS) are provided by the inverse compressibility,

$$\kappa_T^{-1}=\beta\left[\frac{\partial P}{\partial\rho}\right]_T=1+\chi[c] , \tag{4}$$

the potential energy, $u=\beta U/N$,

$$u=\frac{\rho}{2}\int g(r)\beta\phi(r)d\mathbf{r} , \tag{5}$$

and the virial pressure, $Z_v=\beta P/\rho$,

$$Z_v^{ex}=Z_v-1=-\frac{\rho}{2D}\int g(r)r\,\beta\phi'(r)d\mathbf{r} , \tag{6}$$

where the functional $\chi[c]$ is given by

$$\chi[c]=-\rho\int c(r)d\mathbf{r} \tag{7a}$$

or

$$\chi[c]=-\rho\int[c(r)+\beta\phi(r)]d\mathbf{r} \tag{7b}$$

for systems like the OCP that require a compensating background.

The HNC and SMSA EOS's as obtained from the energy or from the virial pressure are identical. Denote by f_v the "virial" excess free energy, $\beta F^{ex}/N$, and let

$$Z_v^{ex}=\rho\left[\frac{\partial f_v}{\partial\rho}\right]_T ,$$

while Z_c^{ex} denotes the corresponding quantity obtained from Eq. (4). The thermodynamic inconsistency of these theories is reflected by $Z_c\neq Z_v$.

Consider also the following functionals of the pair functions:

$$G=\frac{\rho}{2}\int g(r)[c(r)+\beta\phi(r)]d\mathbf{r} , \tag{8}$$

i.e.,

$$G_{\mathrm{SMSA}}=0$$

and

$$G_{\mathrm{HNC}}=\frac{\rho}{2}\int g(r)[g(r)-1-\ln g(r)]d\mathbf{r}\geq 0\ ,$$

$$H=\frac{\rho}{4}\int h^2(r)d\mathbf{r}\geq 0\ , \tag{9}$$

$$L=\frac{1}{2\rho}(2\pi)^{-D}\int d\mathbf{k}\ln[1-\rho\tilde{c}(k)]\ , \tag{10}$$

where the overtilde denotes Fourier transforms,

$$B=\tfrac{1}{2}\{\chi[c]+c(r=0)\}\ , \tag{11}$$

and recall the "Ewald" identity[8,18]

$$u=B+G+\tfrac{1}{2}\ . \tag{12}$$

With the understanding that each functional is evaluated subject to the appropriate closures (2) and (3), the following relations hold for the HNC,[18]

$$f_v=u-G+H+L-\tfrac{1}{2}\ , \tag{13}$$

$$Z_v^{\mathrm{ex}}=\tfrac{1}{2}\chi+H-L+\tfrac{1}{2}\ , \tag{14}$$

and for the SMSA,[18]

$$f_v=u+L-\tfrac{1}{2}+F_0\ , \tag{15}$$

$$Z_v^{\mathrm{ex}}=\tfrac{1}{2}\chi-L+\tfrac{1}{2}\ , \tag{16}$$

where F_0 is a finite constant and $F_0=0$ for potentials having Fourier transforms.

Finally, using the free-energy functionals given by (13) and (15), the HNC and SMSA integral equations can be expressed variationally by

$$\frac{\delta f_v}{\delta c(r)}=0\ . \tag{17}$$

The asymptotic high-density limit (AHDL), denoted by superscript ∞, is the limit in which the compressibility tends to zero. For continuous (soft) potentials it is physically equivalent to the limit in which the excess free energy and the potential energy are both asymptotically equal to the Madelung energy $u_M(\rho)$:

$$f_v^{\infty}=u^{\infty}=\lim_{\rho\to\infty}u=\beta u_M(\rho)\ . \tag{18}$$

A necessary and sufficient condition for the logarithmic term L to be real in the AHDL is

$$\tilde{c}^{\infty}(k)\leq 0 \tag{19}$$

and, consequently,

$$L^{\infty}\geq 0\ . \tag{20}$$

III. THE AHDL-SMSA VARIATIONAL PROBLEM

A. Direct correlation functions and Madelung energy

Inserting (18) into (15) using (3), (8), and (12), the following results are obtained for the SMSA:

$$u^{\infty}=B[c^{\infty}]\ , \tag{21}$$

$$Z_v^{\infty}=\tfrac{1}{2}\chi[c^{\infty}]\ . \tag{22}$$

The AHDL-DCF c^{∞} is obtained [via (17)] by solving the variation equation

$$\frac{\delta B[c]}{\delta c(r)}=0 \tag{23}$$

for continuous functions $c(r)$ which satisfy (19) and the closure (3a). Alternatively, since the SMSA is obtained from the MSA by imposing[18]

$$\frac{\partial f_v}{\partial R}=0\ , \tag{24}$$

we can find c^{∞} by solving (23) for a parametric function (R being the parameter) satisfying (19), (3a), and

$$\frac{\partial B[c]}{\partial R}=0\ . \tag{25}$$

As part of the solution of the AHDL variational problem, we get the asymptotic exclusion region R corresponding to

$$g^{\infty}(r\leq R^{\infty})=0\ . \tag{26}$$

In view of (24) the AHDL of the SMSA must be associated with the singularity for the MSA for the hard-sphere potential, which occurs for total packing fraction, η [$=(\pi/6)\rho R^3$ in three dimensions (3D)], equal to unity: $\eta=1$. Thus a general property of the SMSA is

$$R^{\infty}=2a_{\mathrm{WS}}\ , \tag{27}$$

where a_{WS} [$=(3/4\pi\rho)^{1/2}$ in 3D] is the Wigner-Seitz radius.

From the mapping of the AHDL-HNC on the AHDL-SMSA (Sec. V), we obtain

$$c^{\infty}(r)+\beta\phi(r)>0,\quad r<R^{\infty}\ . \tag{28}$$

Recall the general Ewald-type identity[18]

$$\frac{\rho}{2}\int g(\mathbf{r})\beta\phi(r)d\mathbf{r}=B[\psi]+\frac{\rho}{2}\int g(\mathbf{r})[\psi(r)+\beta\phi(r)]d\mathbf{r}-\tfrac{1}{2}(2\pi)^{-D}\int[1+\rho\tilde{h}(k)]\tilde{\psi}(k)d\mathbf{k}\ , \tag{29}$$

where $\psi(r)$ is any function for which $\tilde{\psi}(k)$ exists. Since the exact PCF $g(r)$ and structure factor $S(k)=1+\rho\tilde{h}(k)$ are non-negative (by definition), the choice $\psi(r)=c^{\infty}(r)$, in view of (19) and (28), ensures that the AHDL-SMSA Madelung energy is an exact lower bound to the true potential energy of the system:

$$u\geq B[c^{\infty}]\ . \tag{30}$$

The AHDL-SMSA variational problem is, in fact, a "best-bound" problem.

B. Green's-function potentials: The OCP

This "best-bound" problem has been solved[23] for Green's-function potentials, $\phi_{\mathrm{GF}}(r)$, satisfying $\tilde{\phi}_{\mathrm{GF}}(k)\geq 0$:

$$\frac{1}{\beta}c^{\infty}_{\mathrm{GF}}(r) \tag{31a}$$

is the ("electrostatic") interaction between two particles of separation r, when their "charge" is smeared uniformly inside a D-dimensional sphere of radius a_{WS} centered on each particle. The MSA for hard spheres was also solved in the AHDL to give[23]

$$\frac{c^{\infty}(r)}{c^{\infty}(0)}\ , \tag{31b}$$

the overlap volume of two spheres of diameter $R=2a_{\mathrm{WS}}$ and separation r divided by the volume of a sphere of diameter $R=2a_{\mathrm{WS}}$, which equals

$$\omega(r,R)=\omega(r/R)\ ,$$

e.g., in 3D,

$$\omega(r/R)=\begin{cases}1-\frac{3}{2}(r/R)+\frac{1}{2}(r/R)^3, & r\le R\\ 0, & r\ge R\ .\end{cases} \tag{32}$$

Defining $x=r/a_{\mathrm{WS}}$ and the uniform smearing function

$$\mu(x)=\begin{cases}1, & |\mathbf{x}|<1\\ 0, & |\mathbf{x}|\ge 1\end{cases}\times\frac{D}{\omega_D}\ , \tag{33}$$

with Fourier transform $\tilde{\mu}(k)$, e.g., in 3D,

$$\tilde{\mu}_{3\mathrm{D}}(k)=3(\sin k-k\cos k)/k^3,\quad \tilde{\mu}(0)=1\ , \tag{34}$$

we obtain

$$\tilde{c}^{\infty}_{\mathrm{GF}}(k)=-\beta(\tilde{\mu}(k))^2\tilde{\phi}_{\mathrm{GF}}(k)\ , \tag{35}$$

$$c^{\infty}_{\mathrm{GF}}(r)=-\beta\frac{\omega_D}{D}\int\phi_{\mathrm{GF}}(|\mathbf{x}-\mathbf{x}'|)\omega(|\mathbf{x}'|/2)d\mathbf{x}'\ , \tag{36}$$

where $\omega_D=(2\pi)^{D/2}/\Gamma(D/2)$ is the surface of a unit D sphere.

For the 3D Coulomb potential (i.e., the OCP), $\beta\phi(r)=\Gamma/x$, we obtain[22(d)]

$$\rho\tilde{c}^{\infty}_{\mathrm{OCP}}(k)=-\frac{27\Gamma}{k^2}\left[\frac{\sin k-k\cos k}{k^3}\right]^2, \tag{37}$$

$$c^{\infty}_{\mathrm{OCP}}(r)=\begin{cases}-\frac{6}{5}\Gamma\left[1-\frac{5}{3}\left[\frac{r}{2a_{\mathrm{WS}}}\right]^2+\frac{5}{4}\left[\frac{r}{2a_{\mathrm{WS}}}\right]^3\right.\\ \qquad\left.-\frac{1}{6}\left[\frac{r}{2a_{\mathrm{WS}}}\right]^5\right], & r\le 2a_{\mathrm{WS}}\\ -\dfrac{1}{2(r/2a_{\mathrm{WS}})}, & r\ge 2a_{\mathrm{WS}}\end{cases} \tag{38}$$

$$u^{\infty}=-\tfrac{9}{10}\Gamma\ , \tag{39a}$$

$$c^{\infty}(r=0)=-\tfrac{6}{5}\Gamma\ , \tag{39b}$$

$$\chi[c^{\infty}]=-\tfrac{6}{10}\Gamma\ , \tag{39c}$$

$$(\kappa_T^{-1})_{\mathrm{virial}}=-\tfrac{4}{10}\Gamma\ , \tag{39d}$$

where the difference between (39c) and (39d) is a manifestation of the thermodynamic inconsistency of the SMSA.

C. Special features of the inverse power potentials

The inverse power potentials $\phi(r)=\epsilon(\sigma/r)^m$, of which the Coulomb is a special case, $m=1$, are homogeneous functions, and thus a single isotherm or a single isochore determines completely the excess thermodynamic properties. Using the reduced length $x=r/a_{\mathrm{WS}}$ we write $\beta\phi(x)=\Gamma/x^m$, where $\Gamma\sim\beta\rho^{m/D}$ is the coupling constant corresponding to the conventional plasma parameter $\Gamma=\beta Q^2/a_{\mathrm{WS}}$ for $m=1$, so that $u(\beta,\rho)=u(\Gamma)$ and $g(r,\beta,\rho)=g(x,\Gamma)$. The AHDL-SMSA solution has the form

$$c^{\infty}(x)=-\Gamma\Psi(x)\ , \tag{40}$$

where the finite and continuous function $\Psi(x)$ satisfies

$$\Psi(x\ge 2)=x^{-m},\quad \Psi(x\le 2)<x^{-m}\ . \tag{41}$$

The thermodynamic functions are given by

$$u^{\infty}=\alpha(m)\Gamma\ , \tag{42a}$$

$$Z_v^{\infty}=\frac{m}{D}\alpha(m)\Gamma\ , \tag{42b}$$

$$c^{\infty}(0)=2\frac{D-m}{D}\alpha(m)\Gamma\ , \tag{42c}$$

$$\chi[c^{\infty}]=\frac{2m}{D}\alpha(m)\Gamma\ , \tag{42d}$$

$$(\kappa_T^{-1})_{\mathrm{virial}}=\frac{m}{D}\left[\frac{m}{D}+1\right]\alpha(m)\Gamma\ , \tag{42e}$$

where $\alpha(m)$ is the Madelung constant. Relations (42b) and (42e) are obtained from (42a) by using the general properties of inverse power systems, namely

$$Z_v^{\mathrm{ex}}=\frac{m}{D}u$$

and

$$(\kappa_T^{-1})_v=1+\frac{m}{D}u+\left[\frac{m}{D}\right]^2\Gamma\frac{du}{d\Gamma}\ ,$$

while (42c) and (42d) then follow directly from (21) and (22). Recall that these relations can be also obtained directly from (42a) and (12) by applying the general differential equation that relates the "virial" and "compressibility" EOS's for the SMSA.[18]

The SMSA properties (42c) and (42d) can be obtained directly from the variational statement (23): The variational property of the solution $c^{\infty}(x)$ implies that the correct solution (i.e., the one with the correct length $x^{\infty}=2$) may be sorted out from the function $\Psi(x)$ when its length unit is scaled, i.e., $\Psi(x)\to\bar{\Psi}(x/x_0)$. The scaled DCF must have [see Eq. (41)] the form

$$c^{\infty}(x)=-\Gamma x_0^{-m}\bar{\Psi}(x/x_0)\ , \tag{43}$$

where $\bar{\Psi}(t)$ is a finite and continuous function satisfying

$$\bar{\Psi}(t\ge 1)=t^{-m},\quad \bar{\Psi}(t<1)<t^{-m}\ .$$

The expression for B then takes the form

$$B[c^{\infty}]=\frac{\Gamma}{2}\left[x_0^{D-m}\int_0^{\infty}\bar{\Psi}(t)d\mathbf{t}-x_0^{-m}\bar{\Psi}(0)\right]\ , \tag{44}$$

where for $m<D$ (e.g., the OCP) we replace the integrand $\overline{\Psi}(t)$ by $\overline{\Psi}(t)-t^{-m}$. Optimizing B with respect to the scale x_0, $\partial B[c^\infty]/\partial x_0=0$, to obtain the correct x^∞, we find

$$(x^\infty)^{-D}=\frac{m}{m-D}\frac{1}{\overline{\Psi}(0)}\int\overline{\Psi}(t)dt\,, \tag{45}$$

where again we replace the integrand $\overline{\Psi}(t)$ by $\overline{\Psi}(t)-t^{-m}$ for $m<D$. This relation is satisfied only when the function $\overline{\Psi}$ is obtained from Ψ by using the correct scale (i.e., x^∞). With the correct x^∞ we switch back to the real length, $x=tx^\infty$, to find that (45) is nothing but

$$\chi[c^\infty]/c^\infty(0)=m/(D-m)\,, \tag{46}$$

which in view of (12) is equivalent to (42c) and (42d). Equation (46) is valid also for $m=\infty$ (the hard spheres), and together with Eq. (19) it was used[23] in order to obtain (31b).

D. AHDL-SMSA Ewald functions

A general way to construct scaling functions of the form (43) is to use, instead of $\overline{\Psi}(t)$, the "Ewald" function

$$f(t)=\left[\overline{\Psi}(t)+\frac{t}{m}\overline{\Psi}'(t)\right]\Big/\overline{\Psi}(0) \tag{47}$$

having the properties

$$f(0)=1,\quad f(t\geq 1)=0,\quad f(t<1)>0\,. \tag{48}$$

Defining

$$W(m)=\int_0^\infty f(t)t^{m-1}dt\,, \tag{49}$$

we obtain, after some algebraic manipulation, the following expressions that hold as they stand for either $m>D$ or $m<D$:

$$\overline{\Psi}(x/x_0)=\frac{1}{W(m)}\int_0^{x/x_0}f(t)t^{m-1}dt\,, \tag{50}$$

$$\overline{\Psi}(0)=1/mW(m)\,, \tag{51}$$

$$B[c^\infty]=\Gamma\left[\frac{x_0^{D-m}DW(D)}{2(m-D)W(m)}-\frac{x_0^{-m}}{2mW(m)}\right], \tag{52}$$

$$(x^\infty)^{-D}=DW(D)\,, \tag{53}$$

$$\alpha(m)=\frac{D(x^\infty)^{-m}}{2m(m-D)W(m)}\,. \tag{54}$$

Note that when $f(t)$ is the customary Ewald function $f(t)=e^{-t^2}$, relation (50) corresponds to the well-known theta-function transformation.[30]

With any Ewald function $f(t)$ having the properties

$$f(t)\geq 0,\quad \tilde{f}(k)\geq 0\,, \tag{55a}$$

or

$$f(t)\geq 0,\quad \tilde{\overline{\Psi}}(k)\geq 0\,, \tag{55b}$$

expression (54) provides an exact lower bound to the true potential energy of the inverse power system,

$$u_{\text{exact}}\geq\alpha(m)\Gamma\,. \tag{56}$$

The AHDL-SMSA variational problem is thus set to find the best such bound (i.e., the optimized Ewald function, one for each potential) among Ewald functions satisfying (55b) and $f(t\geq 1)=0$.

These SMSA-optimized Ewald functions are available (from our general solution for Green's-function potentials) for the D-dimensional Coulomb potentials satisfying $\tilde{\phi}(k)=k^{-2}$. Specifically, for the 3D OCP we use (38) and (47) to get

$$f(t)=1-5t^2+5t^3-t^5\,, \tag{57a}$$

while for the 1D Coulomb potential, $\phi(r)\sim r$, we obtain

$$f(t)=1-t^2\,. \tag{57b}$$

All SMSA Ewald functions satisfy

$$DW(D)=D\int_0^\infty f(t)t^{D-1}dt=2^{-D}\,, \tag{58}$$

they have a quadratic small-t behavior, $f(t)-1=O(t^2)$, and they usually do not obey $\tilde{f}(k)\geq 0$. The hard-sphere overlap volume functions may be considered to represent the $m\to\infty$ limit of the SMSA. Using (32) and (47) with $m=\infty$ we obtain the hard-sphere Ewald functions [which satisfy (58)], e.g. [and see (48)],

$$f_{\text{HS-1D}}(t)=1-t\,, \tag{59a}$$

$$f_{\text{HS-3D}}(t)=1-\tfrac{3}{2}t+\tfrac{1}{2}t^3\,, \tag{59b}$$

$$f_{\text{HS-5D}}(t)=1-\tfrac{15}{8}t+\tfrac{5}{4}t^3-\tfrac{3}{8}t^5\,, \tag{59c}$$

$$f_{\text{HS-2D}}(t)=\frac{2}{\pi}[\arccos t-t(1-t^2)^{1/2}]$$
$$=1-\frac{4}{\pi}t+\frac{2}{3\pi}t^3+\cdots\,. \tag{59d}$$

Unlike the SMSA results for soft potentials, these HS Ewald functions contain only odd powers of t. Having the convolution property $\tilde{f}(k)\sim[\tilde{\mu}(k)]^2$ they satisfy (55a). The property (55a) ensures that each of the functions (59) satisfies (56) for every inverse power potential for the appropriate dimensionality. In contrast to the SMSA functions, the usual Ewald function e^{-t^2} satisfies (55a) and (56) for the inverse power potentials for every dimensionality. The SMSA functions provide, however, much better bounds (see Sec. IV B). The bound (56) represents the structure-independent part of the Ewald summation[30] (or integration). In addition to their significance as representing the AHDL DCF's, the SMSA Ewald functions should have interesting consequences in the context of lattice summations, as generating optimized "theta-type" transformations.

When solving the HNC equation for an inverse power potential in strong coupling, $\Gamma\gg 1$, we expect that the "Ewald" function

$$f(x)=\left[c(x)+\frac{x}{m}c'(x)\right]\Big/c(0) \tag{60}$$

will be a slowly varying function of Γ. This reflects the slow variation of the basic length given, e.g., by the position, x_1, of the first peak of $g(x)$. This feature should be

of help in the numerical solution of the HNC equation. Ng[31] employed this idea, implicitly using the e^{-x^2} Ewald function. It is interesting to note that the "length scale" found by Ng from a numerical fit of his HNC-OCP data compares very suggestively with our expression (53) when evaluated for the e^{-x^2} Ewald function:

$$(x_0)_{\rm Ng}^{-1}=1.08\ , \tag{61a}$$

$$(x^{\infty})^{-1}_{\text{Eq. (53)}}=[\tfrac{3}{2}\Gamma(\tfrac{3}{2})]^{+1/3}=(\tfrac{3}{4}\sqrt{\pi})^{1/3}\cong 1.10 \tag{61b}$$

(compare with the discussion of Gaussian "smearing" in Ref. 26).

IV. PAIR CORRELATION FUNCTION IN THE AHDL

A. General analytic form and the approach to the AHDL

Certain general relations may be established between the PCF $g(r)$ and its Laplace transform (LT). We focus attention on 3D and consider

$$G(s)=\int_0^{\infty} rg(r)e^{-sr}dr\ . \tag{62}$$

The structure factor given by

$$S(k)=1+\rho\tilde{h}(k)=[1-\rho\tilde{c}(k)]^{-1} \tag{63}$$

may be expressed as

$$S(k)=1+\frac{4\pi\rho}{k}\,\mathrm{Im}[G(s=-ik)] \tag{64}$$

by using the relations

$$\tilde{h}(k)=\frac{4\pi}{k}\int_0^{\infty} rh(r)\sin(kr)dr\ , \tag{65}$$

$$h(r)=\frac{1}{2\pi^2 r}\int_0^{\infty} k\tilde{h}(k)\sin(kr)dk$$

$$=\frac{1}{2\pi^2 r}\int_{-\infty}^{\infty} k\tilde{h}(k)\frac{e^{ikr}}{2i}dk\ . \tag{66}$$

The inverse LT of (62) gives

$$rg(r)=\frac{1}{2\pi i}\int_{-i\infty+\delta}^{i\infty+\delta} G(s)e^{sr}ds=\sum_j \text{residues of } G(s)e^{sr} \text{ at poles of } G(s),\ \ s=s_j\ . \tag{67}$$

The pole at $s=0$ gives $g(r)=1$ so that

$$h(r)=\frac{1}{r}\sum_j \text{residues of } G(s)e^{sr} \text{ at poles of } G(s),\ \ s=s_j\neq 0\equiv\sum_j h^{(j)}(r)\ . \tag{68}$$

Since $h(r)$ is real, the poles come in complex-conjugate pairs

$$s_j^{\pm}=-\alpha_j\pm i\beta_j,\ \ \alpha_j,\beta_j\geq 0\ . \tag{69}$$

Denoting the residue of $G(s)$ at the poles $s=s_j$ by

$$B_j=B_j^R\pm iB_j^r\ , \tag{70}$$

and defining

$$\tan\theta_j=-\frac{B_j^R}{B_j^r},\ \ A_j=2B_j^R/\sin\theta_j\ , \tag{71}$$

we write

$$h^{(j)}(r)=A_j e^{-\alpha_j r}\sin(\beta_j r+\theta_j)/r\ . \tag{72}$$

Let us choose the indices j such that $\alpha_j<\alpha_{j+1}$ with

$$s_1^{\pm}=-\alpha_1\pm i\beta_1 \tag{73}$$

denoting the pole nearest the imaginary axis. The asymptotic large-r behavior of $g(r)$ is governed by $h^{(1)}(r)$.

Recall that the SMSA PCF is obtained from that for the corresponding MSA PCF $g(r/R,\beta,\rho,\eta)$ by invoking $\eta(\beta,\rho)$ as obtained from (24). Denoting $\epsilon=1-\eta$, then the limit $\epsilon\to 0$ of the SMSA solution for any potential has the following form in 3D,[23,18]

$$G(s)=G_0(s)+\epsilon^3 G_3(s)+\epsilon^4 G_4(s)+\cdots\ , \tag{74}$$

where s is in $a_{\rm WS}^{-1}$ units[32(a)] and $G_0(s)$ is the leading term in the $\epsilon\to 0$ limit for the MSA (i.e., Percus-Yevick) result for the hard spheres,

$$\lim_{\rho\to\infty} G_{\rm SMSA}(s)=\lim_{\epsilon\to 0} G_{\rm PYHS}(s)\ . \tag{75}$$

The limit $\epsilon\to 0$ of the LT, $G_0(s)$, can be calculated directly from the hard-sphere Ewald function $f(t)$ without resort to the detailed solution of the PY equation. For example (see Appendix A), in 3D we denote

$$\hat{f}(s)=\int_0^{\infty} f_{\text{HS-3D}}(t)te^{-st}dt\ , \tag{76}$$

and find [for s in units of $(2a_{\rm WS})^{-1}$]

$$G_0(s)=\frac{1}{12}\frac{s\hat{f}(s)-1/s}{\hat{f}(s)-\hat{f}(s)}=\frac{1}{12}\frac{s(s+1)}{(s+2)+(s-2)e^s}\ . \tag{77}$$

The poles of $G_0(s)$ give the AHDL of the poles of the SMSA solution $G(s)$:

$$\lim_{\rho\to\infty} s_j^{\pm}=\pm iq_j\ , \tag{78}$$

where the q_j are the zeros of the Fourier transform (FT) of the hard-sphere Ewald function [i.e., the zeros of $\tilde{\mu}(k)$]. Likewise, the residues A_j of $G_0(s)$ give the AHDL limit of those for the SMSA.

The 3D results are as follows: The zeroes of $\tilde{\mu}(k)$ are given by the solutions of the equation

$$\tan(q_j)=q_j \tag{79}$$

and, in particular,

$$q_1=4.493\,406\ldots\ . \tag{80}$$

From Appendix B we obtain [for r in (72) given in units of $a_{\rm WS}$]

$$\lim_{\rho\to\infty} A_j^{\rm SMSA}=\tfrac{2}{3}q_j\frac{1+q_j^2}{q_j^2}\equiv A_j^{\infty} \tag{81}$$

and, in particular,

$$A_1^{\infty}=3.144\ldots . \tag{82}$$

For very small, but nonzero, values of ϵ, we should have

$$\beta_j=q_j+b_j\epsilon^{\tau_j} , \tag{83}$$

$$\alpha_j=a_j\epsilon^{\xi_j}\sim\theta_j , \tag{84}$$

where τ_j and ξ_j are universal constants, independent of the potential.[32] The analytic SMSA solution for the OCP (Sec. VI) gives

$$\tau_j=3 , \tag{85}$$

$$\xi_j=6 , \tag{86}$$

independent of j, with $a_j\sim q_j^6$. The SMSA AHDL solution for the inverse power potentials in 3D is[18,23]

$$\epsilon\sim\Gamma^{-1/6} , \tag{87}$$

which, in view of (86), implies

$$\alpha_j^{\infty}\sim 1/\Gamma . \tag{88}$$

This result is important for the analysis of the AHDL HNC.

The behavior of α_j, and of α_1 in particular, determines the contribution of the functional H to the AHDL-HNC EOS. From (9), (68), and (72) we obtain

$$H=\frac{\rho}{4}\int_0^{\infty}4\pi r^2h^2(r)dr$$

$$=\pi\rho\sum_{i,j}A_iA_j\int_0^{\infty}\sin(\beta_ir+\theta_i)\sin(\beta_jr+\theta_j)e^{-(\alpha_i+\alpha_j)r}dr . \tag{89}$$

The leading contribution in the AHDL is due to the "diagonal" $\sin^2\beta_ir$ terms, so that we finally get

$$H^{\infty}=\lim_{\rho\to\infty}H=\tfrac{3}{16}\sum_j\frac{(A_j^{\infty})^2}{\alpha_j^{\infty}(\Gamma)} . \tag{90}$$

For the SMSA we obtain [in view of (88)]

$$H^{\infty}\sim\Gamma , \tag{91}$$

and we shall consider this result for the HNC in the next section.

Following the analysis of Verlet,[33,31] we expect that the position of the peaks of $S(k)$, $k_j^{\max}$, follows the approximate relations

$$k_j^{\max}\simeq\beta_j,\quad s(k_j^{\max})\sim 1/\alpha_j . \tag{92}$$

The SMSA result for the OCP and the PYHS solution satisfy the following relations (for k and α in units of $a_{\rm WS}^{-1}$):

$$\lim_{\rho\to\infty}k_j^{\max}=q_j,\quad \lim_{\rho\to\infty}S(k_j^{\max})\alpha_j\simeq 1 . \tag{93}$$

As long as α_1 is small but nonzero, the PCF $h(r)$ decays exponentially for large r in a way dominated by the first pole s_1^{+}. In the AHDL, when $\alpha_1\to 0$, which is a singular point for the theory, the solution "blows up": In the SMSA and PYHS the singular point occurs for $\epsilon=0$, where all α_j vanish simultaneously and all poles contribute to $h(r)$ at all distances. This picture, but without the details, has been already discussed by Wertheim[2] in connection to the PYHS. The relation between the stability of the HNC solution for the OCP as determined by α_1 has been discussed by Ng.[31] As we show below, nearly all the details of the AHDL-SMSA apply also to the AHDL-HNC.

B. Madelung energy

The exact analytic solution of the AHDL-SMSA variational "best-bound" problem can be obtained, at present, only for Green's-function potentials. An exact analytic expression for the Madelung energy is available, however, for any potential and for any number of dimensions, via the solution of the corresponding AHDL problem for the hard spheres (i.e., the PYHS result):[23]

$$u^{\infty}=\lim_{\eta\to 1}\left[\tfrac{1}{2}\beta\rho\int g_{\rm PYHS}(r/R,\eta)\phi(r)d\mathbf{r}\right] . \tag{94}$$

By analogy with the 3D calculation in Appendix A, we can relate $G_0(s)$ to $f_{\rm HS}(t)$ for any D, through which the 3D expressions, given below, can be generalized.

In 3D we write

$$\phi(r)=\frac{1}{r}\int_0^{\infty}\hat{\phi}(s)e^{-sr}ds , \tag{95}$$

and using (62) and (94), we obtain

$$u_{\rm SMSA}^{\infty}=\frac{\beta}{(2a_{\rm WS})^2}\int_0^{\infty}G_0(s)\hat{\phi}(2sa_{\rm WS})ds . \tag{96}$$

In particular, for the inverse power potentials ($m>D$), we obtain, for the Madelung constant,

$$\alpha(m)=\frac{1}{2^m(m-D)}\int_0^{\infty}\frac{(s+2)s^{m-1}}{(s+2)+(s-2)e^s}ds , \tag{97}$$

while for the OCP ($m=1$), we get

$$\alpha(1)=6\lim_{s\to 0}\left[G_0(s)-\frac{1}{s^2}\right]=-\tfrac{9}{10} . \tag{98}$$

The results in one dimension are special because

$$u_{\rm SMSA}^{\infty}=u_{\rm exact}^{\infty}\ \text{ in 1D} . \tag{99}$$

In 1D we define

$$\phi(r)=\int_0^{\infty}\hat{\phi}(s)e^{-sr}ds , \tag{100}$$

and obtain the general result

$$u_{\rm SMSA}^{\infty}=\rho\int_0^{\infty}\frac{\hat{\phi}(s\rho)}{e^s-1}ds , \tag{101}$$

which takes the following form for the inverse power potentials:

$$u^{\infty}=\left[\frac{1}{\Gamma(m)}\int_0^{\infty}\frac{s^{m-1}}{e^s-1}ds\right]\rho^m\equiv\zeta(m)\rho^m\ . \tag{102}$$

As easily recognized by (102), the expression (101) represents the lattice sum for the 1D equally spaced lattice with nearest-neighbor distance $a_{\rm WS}=1/\rho$. Indeed, using (100) we may write

$$u^{\infty}=\int_0^{\infty}\frac{\hat{\phi}(t)dt}{e^{t/\rho}-1}=\sum_{j>0}\int_0^{\infty}\hat{\phi}(t)e^{-a_{\rm WS}jt}dt$$

$$=\sum_{j>0}\phi(a_{\rm WS}j)=\tfrac{1}{2}\sum_{j\neq 0}\phi(a_{\rm WS}|j|)\ . \tag{103}$$

For the 1D Coulomb potential we find

$$\alpha(1)=-2\lim_{s\to 0}\frac{\partial}{\partial s}\left[\frac{1}{e^s-1}-\frac{1}{s}\right]=-\tfrac{1}{6}\ , \tag{104}$$

in agreement with the "ion-sphere" Onsager bound.[22(d),24,34]

In view of the discussion in Sec. III D, it is instructive to compare the Madelung constants for the inverse power potentials as obtained from different Ewald functions with the fcc lattice sum. The SMSA exact bounds $\alpha(m)$ are obtained from (97), while we use (54) to get the Madelung constants corresponding to $f_{\rm OCP}(t)$ [Eq. (56)], $f_{\rm HS}(t)$ [Eq. (59a)], and e^{-t^2}, i.e., $\alpha_{\rm OCP}$, $\alpha_{\rm HS}$, and α_E, respectively:

$$\alpha_{\rm OCP}=\frac{(m+2)(m+3)(m+5)}{10(m-3)2^{m+1}}\ , \tag{105}$$

$$\alpha_{\rm HS}=\frac{10(m+1)}{(m+2)(m+5)}\alpha_{\rm OCP}\ , \tag{106}$$

$$\alpha_E=\frac{3[\frac{3}{2}\Gamma(\frac{3}{2})]^{m/3}}{2m(m-3)[\Gamma(m/2)/2]}\ . \tag{107}$$

The results in Table I show the better performance of the SMSA and HS Ewald functions as compared with e^{-t^2}. An interesting result is the striking agreement between $\alpha_{\rm OCP}$ and the fcc lattice sums for inverse power potentials $m\lesssim 12$. The SMSA bounds become less effective as m increases.

V. THE AHDL OF THE HNC THEORY FOR SOFT POTENTIALS

We are interested in solutions of the HNC integral equation obtained from (1) and (2) for potentials $\phi(r)$ that are strongly repulsive at short distances. The HNC-PCF $g(r)$ of interest obeys $g(r)\geq 0$, $g(r=0)=0$, $g(r\to\infty)=1$, and the function $g(r)-1-\ln g(r)$ is represented by "scallops" with possible peaks when $g(r)$ is either large or small [i.e., $-\ln g(r)$ is large] and is zero for $g(r)=1$. With r_0 denoting the first such zero, we write

$$c(r)=c_0(r)+c_1(r)\ , \tag{108}$$

where

$$c_0(r)=\begin{cases}-\beta\phi(r), & r>r_0\\ c(r), & r\leq r_0\end{cases} \tag{109}$$

and

$$c_1(r)=\begin{cases}0, & r\leq r_0\\ g(r)-1-\ln g(r)\geq 0, & r\geq r_0\end{cases} \tag{110}$$

are continuous functions. Note that $c_0(r)$ has a SMSA form [compare with (3)], and we must have

$$g(r)<1 \quad \text{for } r<r_0\ . \tag{111}$$

In the AHDL we have

$$\lim_{\rho\to\infty}g(r)=g^{\infty}(r)=0 \quad \text{for } r\leq r_0^{\infty}\ , \tag{112}$$

where

$$r_0^{\infty}=\lim_{\rho\to\infty}r_0\equiv x_0^{\infty}a_{\rm WS} \tag{113}$$

[see (124) below].

We define

$$\chi_1=-\rho\int_{r\geq r_0}[g(r)-1-\ln g(r)]d\mathbf{r}\ , \tag{114}$$

$$G_1=\frac{\rho}{2}\int_{r\geq r_0}g(r)[g(r)-1-\ln g(r)]d\mathbf{r}\ , \tag{115}$$

$$G_0=\frac{\rho}{2}\int_{r\leq r_0}g(r)[c_0(r)+\beta\phi(r)]d\mathbf{r}\ , \tag{116}$$

so that

$$G=G_0+G_1\ , \tag{117}$$

$$B[c]=B[c_0]+\tfrac{1}{2}\chi_1\ , \tag{118}$$

and (12)–(14) take the form

$$u=B[c_0]+G_0+(\tfrac{1}{2}\chi_1+G_1)+\tfrac{1}{2}\ , \tag{119}$$

$$Z_v^{\rm ex}=\tfrac{1}{2}\chi[c_0]+(\tfrac{1}{2}\chi_1+H)-L+\tfrac{1}{2}\ , \tag{120}$$

$$f_v=B[c_0]+(H+\tfrac{1}{2}\chi_1)+L-\tfrac{1}{2}\ . \tag{121}$$

Note that in view of (112) we have

TABLE I. Madelung energies for inverse power potentials in 3D (see the text). The last three columns represent exact lower bounds for u/Γ.

m	$\alpha_{\rm fcc}$	$\alpha_{\rm OCP}$	$\alpha_{\rm SMSA}$	$\alpha_{\rm HS}$	α_E
1	−0.895 929	−0.9	−0.9	−1.0	−0.9305
4	1.181 98	1.181 25	1.171	1.093 75	1.096 25
6	0.205 95	0.206 25	0.197 86	0.164 06	0.1473
9	0.030 05	0.030 08	0.0267	0.019 53	0.0112
12	0.004 926	0.004 842	0.003 913	0.002 645	0.000 723

$$G_0^\infty = \lim_{\rho\to\infty} G_0 = 0 \ . \tag{122}$$

To simplify expressions, we define $x = r/a_{\rm WS}$ and proceed with the analysis as applied to inverse power potentials $\beta\phi(r) = \Gamma/x^m$. The Madelung behavior in the AHDL implies

$$c_0^\infty(x,\Gamma) = \lim_{\Gamma\to\infty} c_0(x,\Gamma) = -\Gamma\psi_{\rm HNC}(x) \ , \tag{123}$$

where

$$\psi_{\rm HNC}(x) \le x^{-m} \ , \tag{124a}$$

$$\psi_{\rm HNC}(x) = x^{-m}, \quad x \ge x_0^\infty \tag{124b}$$

and it is the inequality (124a), i.e., the inequality in (2), which gives (112), i.e.,

$$g^\infty(x \le x_0^\infty) = \lim_{\Gamma\to\infty} e^{-\Gamma[x^{-m}+\psi_{\rm HNC}(x)]} = 0 \ . \tag{124c}$$

To have the mapping of the AHDL-HNC on the AHDL-SMSA, i.e.,

$$x_0^\infty = x_{\rm SMSA}^\infty = 2 \ , \tag{125}$$

$$\psi_{\rm HNC}(x) = \psi_{\rm SMSA}(x) \ , \tag{126}$$

which then implies that (124a) also holds for the SMSA, we must have the following HNC properties:

$$\lim_{\Gamma\to\infty} c_1(x,\Gamma)/\Gamma = \lim_{\Gamma\to\infty} \frac{g(x,\Gamma)-1-\ln g(x,\Gamma)}{\Gamma}\bigg|_{x\ge x_0^\infty} = 0 \ , \tag{127}$$

$$\lim_{\Gamma\to\infty} u = u^\infty = B[c_0^\infty] \ , \tag{128}$$

$$\lim_{\Gamma\to\infty} Z_v^{\rm ex} = Z_v^\infty = \tfrac{1}{2}\chi[c_0^\infty] \ . \tag{129}$$

In Ref. 23 we started with the assumption

$$\lim_{\Gamma\to\infty} (G/\Gamma) = 0 \quad \text{(case A)} \ , \tag{130}$$

and it readily followed that in view of (112) and the inequality in (110) we get (127). In turn, in view that $H^\infty \ge 0$ and $L^\infty \ge 0$ we should, because of (18), also get (128) and (129).

The analysis in Sec. IV A and, in particular, the SMSA result $H^\infty \sim \Gamma$, prompts us to consider also the possibility

$$\lim_{\Gamma\to\infty} (G/\Gamma) = a_G > 0 \quad \text{(case B)} \ , \tag{131}$$

with $a_G = \text{const}$. Dominant AHDL contributions to G can come from either terms of the type $g_{\rm max}^2\Delta$ or from the long-range decay of $h(r)$. Δ is the width of the first peak and $g_{\rm max}$ is its height. Considering the energy integral

$$u = \tfrac{3}{2}\Gamma\int_0^\infty g(x,\Gamma)x^{-m}x^2dx \ , \tag{132}$$

then, in view of the Madelung behavior $u^\infty = \alpha(m)\Gamma$, we must have

$$\lim_{\Gamma\to\infty} g_{\rm max}\Delta = \text{const} \ . \tag{133}$$

Let us now first assume that (127) holds. Then, from (133), we find that the constant $a_G = G^\infty/\Gamma$ of (131) must originate from the long-range nature of $h(r)$. Indeed, for small $h(r)$ we have

$$G = \frac{\rho}{2}\int g(r)[g(r)-1-\ln g(r)]d\mathbf{r} \cong \frac{\rho}{4}\int h^2(r)d\mathbf{r} = H \ , \tag{134}$$

and the $1/\Gamma$ behavior of α_1 [Eq. (88)] is responsible for (131). A specific expression for H is thus given by (90). Equation (134), i.e.,

$$a_G = G^\infty/\Gamma = \lim_{\Gamma\to\infty}(G/\Gamma) = \lim_{\Gamma\to\infty}(H/\Gamma) = H^\infty/\Gamma = a_H \ , \tag{135}$$

immediately implies [in view of (18) and (13)]

$$\lim_{\Gamma\to\infty}(L/\Gamma) = L^\infty/\Gamma = 0 \ . \tag{136}$$

The above situation that leads to (134) also yields

$$\tfrac{1}{2}\chi_1^\infty = \lim_{\Gamma\to\infty} -\frac{\rho}{2}\int g(r)[g(r)-1-\ln g(r)]d\mathbf{r} = -H^\infty \ , \tag{137}$$

so that from (119) and (120) we finally obtain the desired results (128) and (129).

On the other hand, let us start from the discussion in Sec. IV, from which we have that

$$a_H = H^\infty/\Gamma \tag{138}$$

originates from the long range of $h(r)$. It then follows that

$$\lim_{\Gamma\to\infty}(h_{\rm max}^2\Delta/\Gamma) = \lim_{\Gamma\to\infty}(g_{\rm max}^2\Delta/\Gamma) = 0 \tag{139}$$

and [in view of (133)]

$$\lim_{\Gamma\to\infty}[g(x,\Gamma)/\Gamma] = 0 \ . \tag{140}$$

Since $\lim_{g\to 0}(g\ln g) = 0$, then we also obtain (135). From (135) and (134) we may consider the short-range (SR) contribution to G,

$$\lim_{\Gamma\to\infty}(G_{\rm SR}/\Gamma) = \lim_{\Gamma\to\infty}\frac{D}{\omega_D 2} \times \int_{x<x_L<\infty}\frac{g(x)}{\Gamma}[g(x)-1-\ln g(x)]d\mathbf{x} = 0 \ . \tag{141}$$

Since in the HNC theory both $g(x)$ and $g(x)-1-\ln g(x)$ are non-negative, the only possibility of satisfying (141) is by use of (127).

In either case A, Eq. (130), or case B, Eq. (131), for which we need (127), our analysis predicts that (125)–(129) and (also see Ref. 23) (74)–(85) are all valid for the AHDL-HNC as well as the AHDL-SMSA. For case B we also obtain (86)–(91). Note, however, that the coefficients b_j and a_j in (83) and (84) need not be the same for the HNC and the SMSA. The HNC ϵ expansion is obtained by inverting the relation $x_0(\Gamma)$ and using it to express the HNC solution in terms of x_0 while using (in

3D) $\epsilon=1-(x_0/2)^3$. r_0 is the HNC analogue of the SMSA parameter R. This expected general similarity of the HNC and SMSA suggests, in view of the SMSA result (88), that case B, namely $\alpha_j \sim 1/\Gamma$, is the actual HNC behavior.

Thus, the virial (energy) EOS of the HNC and SMSA theories are identical in the AHDL:

$$u^{\infty}_{\mathrm{HNC}} = u^{\infty}_{\mathrm{SMSA}} , \tag{142a}$$

in general, and

$$\alpha^{(m)}_{\mathrm{HNC}} = \alpha^{(m)}_{\mathrm{SMSA}} , \tag{142b}$$

for the inverse power potentials. There is a difference in the compressibility EOS due to the contribution of χ_1 to the HNC $\beta(\partial P/\partial\rho)_T$:

$$\beta\left[\frac{\partial P}{\partial\rho}\right]^{\infty}_T = \chi[C_0^{\infty}]+\chi_1^{\infty} = \frac{2m}{D}\alpha(m)\Gamma - 2a_H\Gamma , \tag{143}$$

where $\alpha(m)$ is the HNC (SMSA) Madelung constant. It is of interest to investigate whether for some $m > D$ (in view of the above expression) the HNC inverse compressibility vanishes, for a purely repulsive potential, at some finite $\Gamma=\Gamma_c$.

It should be noted that we could not find anything in the SMSA theory that would imply (28) *a priori*. In order to obtain it, we needed the mapping on the AHDL-HNC. From its relation to the Onsager bounds for Green's-function potentials, we know that the AHDL-SMSA does obey (28), and (30) always holds in practice. This may be of help in a search for a rigorous proof of (127).

VI. HNC AND SMSA THEORIES FOR THE OCP

A. Exact analytic solution of the SMSA

The exact solution of the MSA for charged hard spheres in a uniform neutralizing background was given by Palmer and Weeks (PW).[29] With r in units of the hard-sphere diameter d, $d/a_{\mathrm{WS}}=2\eta^{1/3}$, $\gamma=\Gamma/2\eta^{1/3}$, $\kappa=(24\eta\gamma)^{1/2}$, the OZ equation (2) was solved for the MSA closure $c(r<1)=-\gamma/r$ and $g(r<1)=0$. The solution, quoted in Appendix C, also gives the PYHS results[2] upon taking the limit $\gamma=0$ for fixed η. The SMSA is obtained from the MSA solution by equating the linear term in $c(r<1)$ to zero, i.e., $M=0$ in Appendix C. The resulting function $\epsilon(\Gamma)=\eta(\Gamma)-1$ has the following AHDL expansion:[35]

$$\epsilon(\Gamma)=\left[\frac{108}{\Gamma}\right]^{1/6}-\frac{1}{3}\left[\frac{108}{\Gamma}\right]^{1/3}+\frac{5}{108}\left[\frac{108}{\Gamma}\right]^{1/2}-\frac{1}{243}\left[\frac{108}{\Gamma}\right]^{2/3}+\cdots . \tag{144}$$

Inserting this expansion into the MSA expression for the potential energy, Eq. (C9) in Appendix C, we obtain[35]

$$u(\Gamma)=u_{\mathrm{MSA}}(\eta(\Gamma),\Gamma) = -\tfrac{9}{10}\Gamma+3\left[\frac{\Gamma}{108}\right]^{1/2}+\frac{1}{15}\left[\frac{\Gamma}{108}\right]^{1/6}+O(\Gamma^{-1/6}) . \tag{145}$$

The AHDL expansion for the other thermodynamic quantities readily follows from (11), (12), (15), and (16).

In order to see the connection between the PW solution and our general result (31a), take the limit $\gamma\to\infty$ for fixed $\eta<1$, and obtain from the PW DCF the following expression:

$$-\frac{c^{\infty}(r)}{\gamma}=\lim_{\gamma\to\infty}-\frac{c(r)}{\gamma}\equiv\psi(r)=\begin{cases}\psi^{<}(r), & r\le 1\\ 1/r, & r\ge 1\end{cases} \tag{146}$$

$$\psi^{<}(r)=\left[2+\frac{2\eta^2}{5}\right]-(1-\eta)^2 r-4\eta r^2+(2\eta+\eta^2)r^3-\tfrac{2}{5}\eta^2 r^5 . \tag{147}$$

Note that $\psi(r)$ can be written as

$$\psi(r)=\psi_{vv}(r)+\psi_{ss}(r)+\psi_{vs}(r) , \tag{148}$$

where, for $r\le 1$,

$$\psi_{vv}(r)=\eta^2(\tfrac{12}{5}-4r^2+3r^3-\tfrac{2}{5}r^5) , \tag{149a}$$

$$\psi_{ss}(r)=(1-\eta)^2(2-r) , \tag{149b}$$

$$\psi_{vs}(r)=\eta(1-\eta)(4-4r^2+2r^3) . \tag{149c}$$

These functions are (respectively) the volume-volume, surface-surface, and volume-surface electrostatic interactions between two spheres of diameter 1, each having a charge $1-\eta$ uniformly spread on the surface and a charge η uniformly spread in the volume. This result for the charged hard spheres is a special case of our general solution[23,28] of the AHDL for hard objects with embedded charge distributions associated with arbitrary Green's-function potentials. The limit $\gamma\to\infty$ for fixed $\eta<1$ in the energy expression gives

$$u^{\infty}(\eta,\Gamma)=-\left[1+\eta-\frac{\eta^2}{5}\right]\gamma=-\frac{1+\eta-\eta^2/5}{2\eta^{1/3}}\Gamma , \tag{150}$$

which is easily recognized as representing the Onsager[24] energy of the system of charged spheres described above. This simple electrostatic interpretation of the PW solution is also a special case of our general result for charged objects.[23,28] To see the role of (24), note that $\partial u^{\infty}(\eta,\Gamma)/\partial\eta\,|_{\Gamma}$ gives $\eta^{\infty}=1$ and $u^{\infty}=-0.9\Gamma$. With $\eta=1$, Eqs. (146) and (150) give (38) and (39).

Detailed analytical investigation of the pole structure of the PW $G(s)$ involves very tedious algebra in view of the ϵ^6 dependence of α_i. This means dealing with expansions up to at least sixth order. From the *nature* of the expansions we could establish, however, that the SMSA-OCP obeys the following type of scaling when we use the SMSA $\epsilon(\Gamma)$ to express the structure in terms of ϵ only:

$$\alpha_i=f_{\alpha}(q_i,\epsilon)=a_{\alpha_i}\epsilon^6+\cdots , \tag{151a}$$

$$\beta_i=f_{\beta}(q_i,\epsilon)=q_i-q_{\beta_i}\epsilon^3+\cdots , \tag{151b}$$

$$\theta_i\cong O(\epsilon^6) , \tag{151c}$$

$$a_{\alpha_i}\cong O(q_i^6) , \tag{151d}$$

$$A_i=\tfrac{2}{3}q_i\frac{1+q_i^2}{q_i^2}+a_{A_i}\epsilon^3+\cdots , \tag{151e}$$

where f_α and f_β are universal (independent of j) functions of q_i and ϵ. The detailed analysis was performed numerically by calculating the poles of $G(s)$ and its residues as functions of ϵ and Γ. This is why we cannot quote exact numbers for the coefficients $a_{\alpha_i}, a_{\beta_i}, a_{A_i}$. Approximate numbers can be obtained from the figures in the next section.

B. Comparison between the SMSA and HNC theories for the OCP

In this subsection we compare the results from the analytic solution of the SMSA with those obtained from the numerical solution of the HNC for the OCP (up to $\Gamma=7000$) as obtained by Ng.[31] We first list the features and numbers which (according to our analysis above) should be the same for both HNC and SMSA, and for which the HNC data are *available*:[31]

$$\alpha_1 \to O(\Gamma)\,, \tag{152a}$$

$$\beta_1 \to 4.4934\ldots + O(\Gamma^{-1/2})\,, \tag{152b}$$

$$A_1 \to 3.144\ldots + O(\Gamma^{-1/2})\,, \tag{152c}$$

$$x_0, x_1 \to 2 + O(\Gamma^{-1/6})\,, \tag{152d}$$

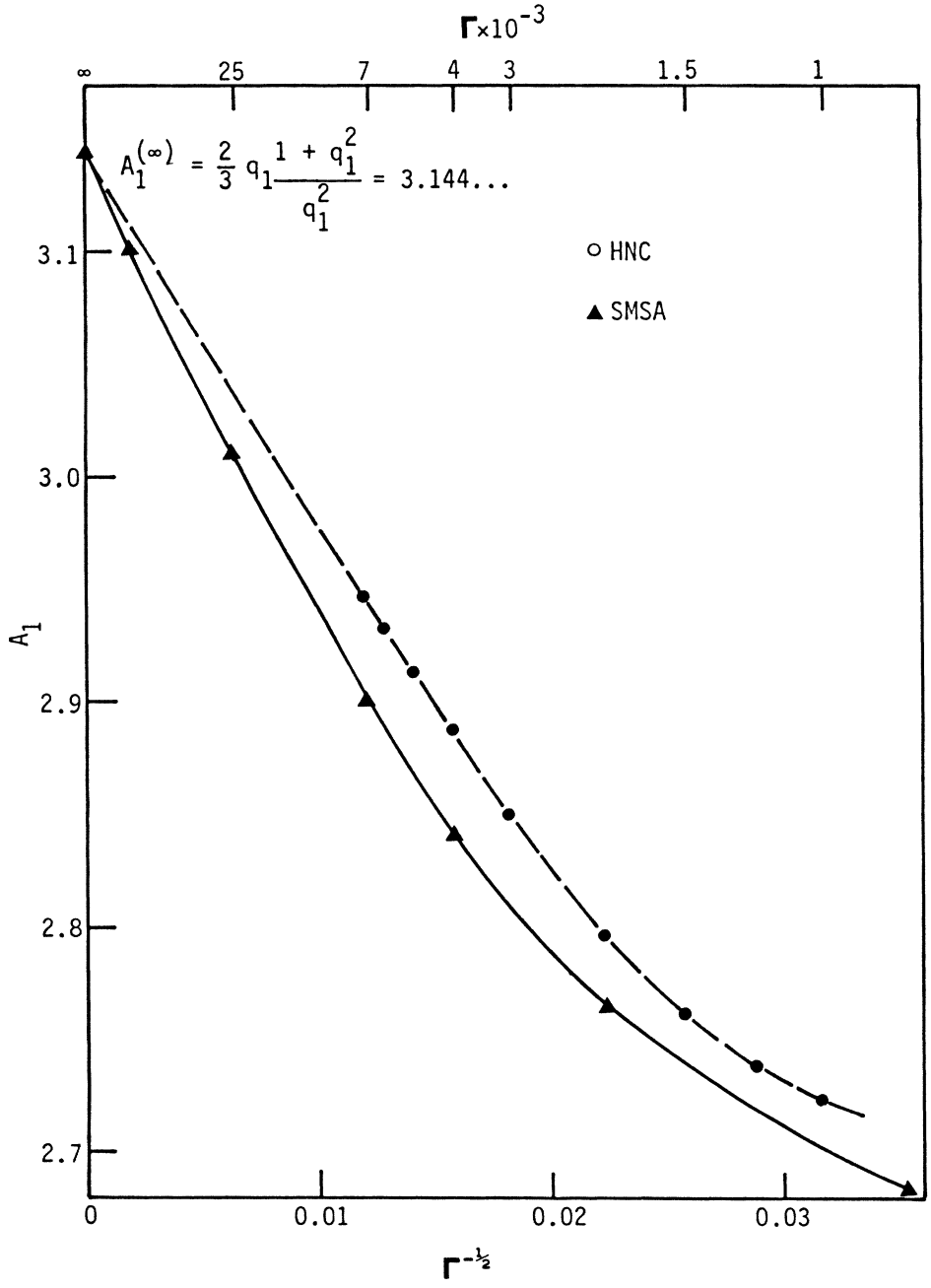

FIG. 1. Residue of $G(s)$ at first nonzero pole (see text). The HNC data are from Table III of Ng (Ref. 31), and the line serves only to guide the eye.

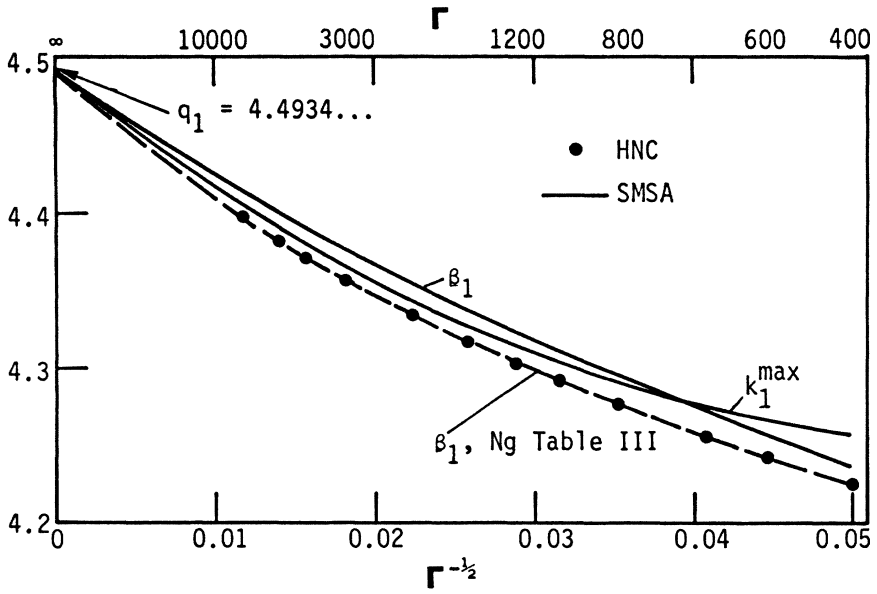

FIG. 2. Imaginary part of first nonzero pole of $G(s)$, β_1, and position of first peak of $S(k)$, k_1^{max} (see text). The HNC data are from Table III of Ng (Ref. 31), and the line serves only to guide the eye.

$$u \to -0.9\Gamma + O(\Gamma^{1/2}) , \tag{152e}$$

$$c(0) \to -1.2\Gamma + O(\Gamma^{1/2}) , \tag{152f}$$

where x_1 is the position of the first peak of the PCF $g(x,\Gamma)$, and x_0 is the position of the first zero of the HNC $g(x) - 1 - \ln g(x)$. The results presented in Figs. 1–6 are in complete agreement with our predictions. Bearing in mind the interconnections between these many predicted qualities, the way they are borne out by the comparison in the figures can leave little doubt as to their validity. The reason for this appeal to the numerical data is the fact that our analysis is not strictly rigorous in the mathematical sense, and highly nonlinear equations may have surprises in store.

Finally, with the help of Fig. 3, we can now estimate the HNC-AHDL correction to the SMSA compressibility

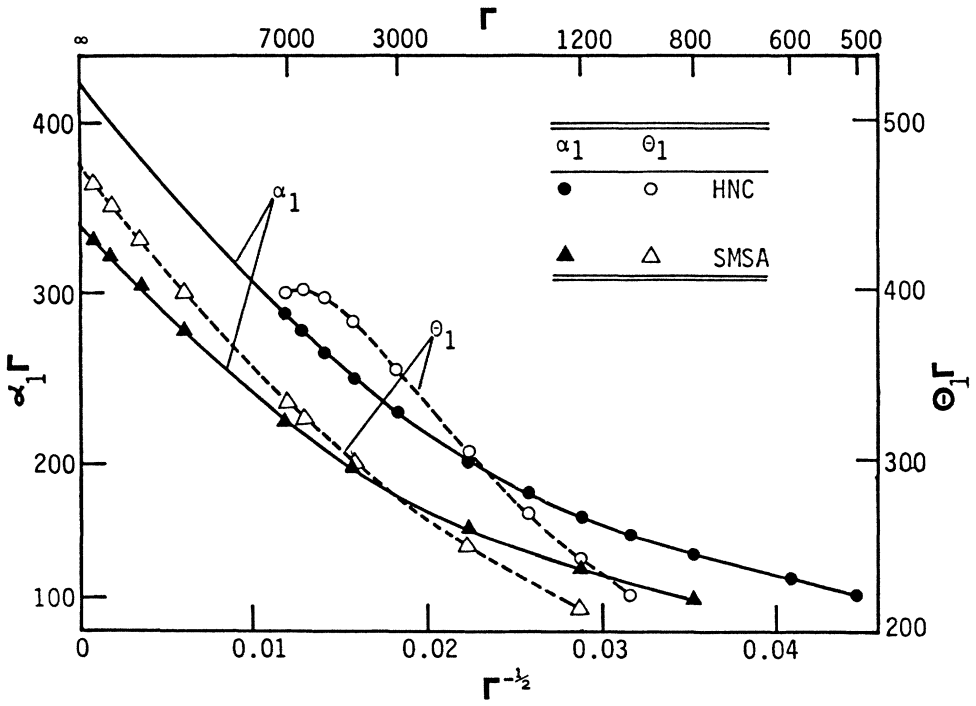

FIG. 3. Real part of the first nonzero pole of $G(s)$, α_1, and "phase shift" θ_1 (see text). The HNC data are from Table III of Ng (Ref. 31), and the line serves only to guide the eye.

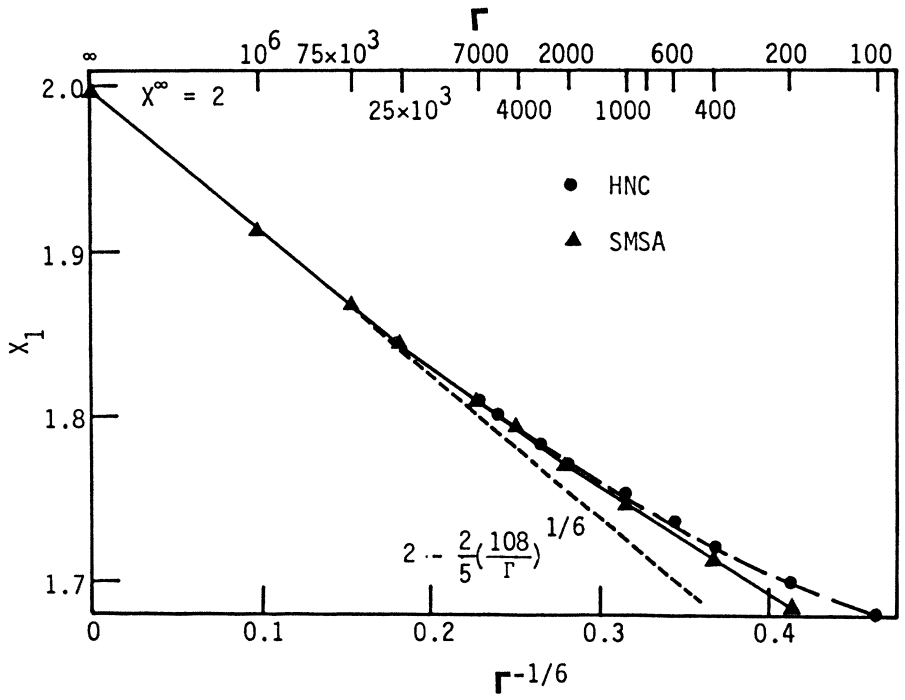

FIG. 4. Position of the first peak of $g(x)$, x_1 (see text). The HNC data are taken from Ng (Ref. 31), and the line serves only to guide the eye.

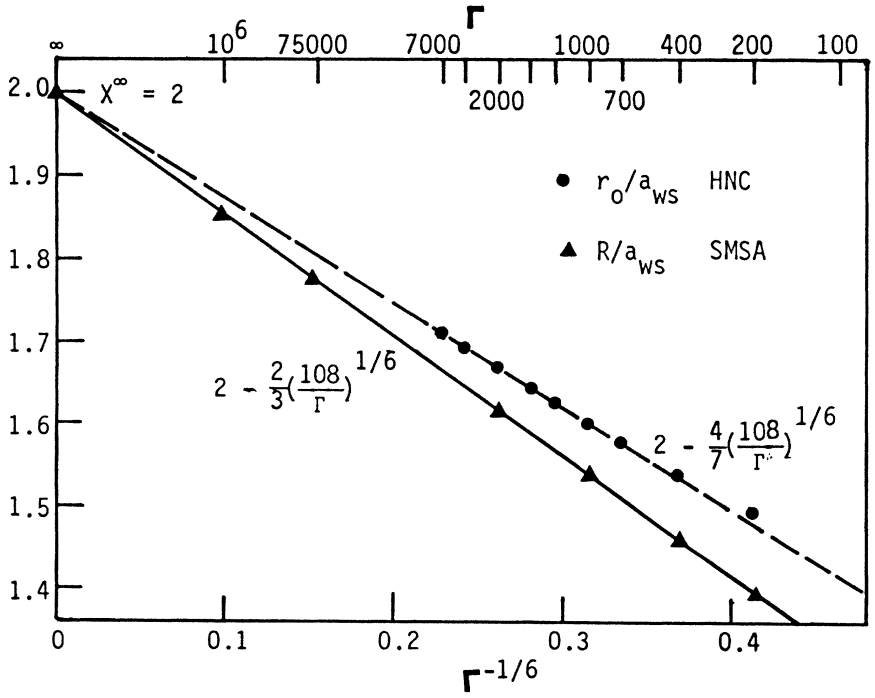

FIG. 5. Position of the first zero of the HNC $g(x)-1-\ln g(x)$, x_0, and the hard-core parameter for the SMSA, R. The HNC data are from Ng (Ref. 31), and the lines serve only to guide the eye.

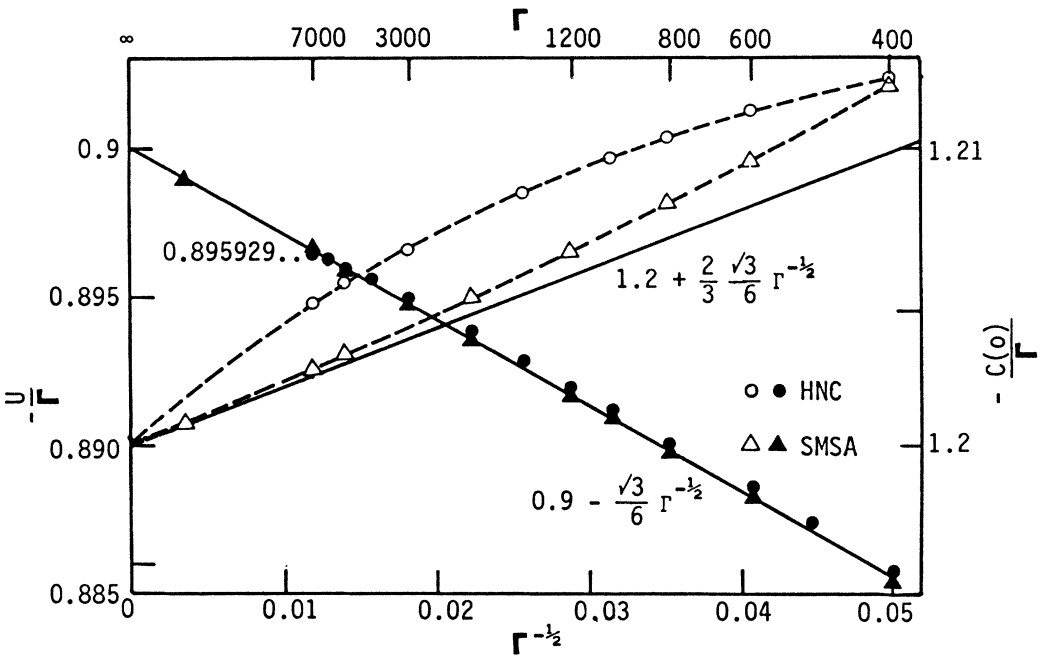

FIG. 6. Potential energy u and value of DCF at the origin, $c(0)$ (see text). The HNC data are taken from Ng (Ref. 31), and the lines serve only to guide the eye.

EOS. From Fig. 3 we find

$$(\alpha_1)_{\mathrm{SMSA}} \sim \tfrac{3}{4}(\alpha_1)_{\mathrm{HNC}} \rightarrow 340/\Gamma \ . \tag{153}$$

From (90) and (151) we find, for the SMSA,

$$(2a_H)_{\mathrm{SMSA}} \cong \frac{3}{8}\frac{(A_1^{\infty})^2}{\Gamma\alpha_1^{\infty}} \sum_{j\geq 1}\left[\frac{q_1}{q_j}\right]^4 \cong 0.013 \ , \tag{154}$$

so that the HNC result is estimated by

$$(2a_H)_{\mathrm{HNC}} \cong 0.011 \ . \tag{155}$$

Unfortunately, Ng[31] did not present results of the HNC compressibility EOS. Our estimate (155) is in good agreement with more recent unpublished HNC data.[36(a)]

The main difference between the HNC and SMSA results for the OCP is the general shape of the PCF $g(r)$. The HNC $g(r)$ is always non-negative, while that for the SMSA attains negative values for large Γ starting at $\Gamma \sim 400$. The SMSA result lacks all the interesting features discussed by Ng.[31] These points will be discussed elsewhere.

C. Comments on the numerical analysis of the HNC data

The general similarity between the AHDL-HNC and the AHDL-SMSA results for the OCP, in full agreement with our general analysis of these theories, sheds light on the problematics associated with the direct numerical analysis of the HNC data when performed without resort to basic theoretical analysis. To be specific, consider the two quantities $u(\Gamma)$ and $x_1(\Gamma)$, which are expected to give $\lim_{\Gamma\to\infty} u(\Gamma)/\Gamma = -0.9$ and $\lim_{\Gamma\to\infty} x_1(\Gamma) = 2$. For the sake of argument, we assume that the HNC data, for $\Gamma < 7000$, is of absolute accuracy (i.e., exact).

(a) Ng[31] fitted $u(\Gamma)$ for $100 < \Gamma < 6000$ by several different polynomials and rational functions of various inverse powers of Γ with three to six parameters, with the obvious leading behavior $a_1\Gamma + a_2\Gamma^{1/2}$. All his numerical fits indicates that $u(\Gamma)$ is a very smooth function of Γ in that region with a limiting value of $(-0.8995 \pm 0.0002)\Gamma$. It is to be noted that inserting in such fitting schemes the SMSA values instead of the HNC results, we also cannot retrieve the exact value of -0.9 unless we use the exact AHDL expansion form and we maintain an appropriate number of terms (depending on the range of values for Γ). In Table II we compare the HNC and SMSA results and

TABLE II. HNC and SMSA potential energies for the OCP. The HNC data for $\Gamma > 200$ are from Ng (Ref. 31) and those for $\Gamma \leq 200$ are from Ref. 36(b).

Γ	$\frac{u_{\mathrm{SMSA}} - u_{\mathrm{HNC}}}{\Gamma}$	Γ	$\frac{u_{\mathrm{SMSA}} - u_{\mathrm{HNC}}}{\Gamma}$
0	0	200	0.000 041
0.01	0.0001	400	0.000 392
0.05	0.0022	600	0.000 433
0.1	−0.001	800	0.000 413
1	−0.037	1000	0.000 378
5	−0.019 27	1200	0.000 344
10	−0.011 76	2000	0.000 237
40	−0.003 14	3000	0.000 151
60	−0.001 83	4000	0.000 090
80	−0.001 25	5000	0.000 040
100	−0.000 794	6000	0.000 004

find no indication (in the general trend of the difference) that $\lim_{\Gamma\to\infty}(u_{\rm HNC}-u_{\rm SMSA})/\Gamma\neq 0$.

(b) The general difficulty associated with the asymptotic nature of the expansion is much more pronounced in the case of $x_1(\Gamma)$. In Fig. 7 we present the data of Fig. 4, but on the $\Gamma^{-1/2}$ scale. It is evident that in the region $\Gamma<6000$ both the SMSA and HNC data suggest a fit of the form $C_1+C_2\Gamma^{-1/2}$, with $C_1\sim 1.8$, in contrast to the correct picture given by Fig. 4.

(c) Finally, any method of numerical solution of the HNC (and for that matter, of the SMSA as well) must encounter, as $\Gamma\gg 1$, the problem associated with $\alpha_1\to 0$. Any numerical method can work only in a finite region of x, $x<R_c$. When the true α_1 approaches the value $\alpha_1\sim 1/R_c$, the truncation error makes the solution unreliable. Ng used a 4096-point mesh with separation $\Delta x=0.025$, i.e., $R_c\sim 100$. Considering Fig. 3, we expect his results for $\Gamma<6000$ to be accurate, while his scheme must break around $\Gamma\sim 30\,000$. This is still a relatively small Γ if we consider the behavior of x_1 in Fig. 7.

VII. SUMMARY AND IMPLICATIONS

We continued the line of study of Ref. 23 and considered aspects of the SMSA, HNC, and PYHS theories. We found that they all share the same AHDL $G_0(s)$, with similar pole structure that determines the EOS in strong coupling. The scaling properties of the inverse power potentials as borne out by the AHDL-SMSA variational problem led to the introduction and analysis of the SMSA Ewald functions. The relation between the SMSA Ewald functions and the AHDL analytic structure of the SMSA, HNC, and PYHS theories was considered, and the special role played by the PYHS (overlap volume) Ewald functions was clarified. Detailed analysis of the relation between the HNC and SMSA theories in the AHDL, and of the significance of the $1/\Gamma$ dependence of α_j, was presented. The comparison of the analytic SMSA results and the numerical HNC data for the OCP provided an illustration for the general picture.

Generalizing our results (in view of Sec. VI in Ref. 23), we expect the following universal AHDL behavior of the HNC and SMSA theories for soft interactions:

$$\beta_j-q_i\sim\epsilon^{(D+3)/2}\sim\Gamma^{-(D+3)/[3(D+1)]}\,, \tag{156a}$$

$$\alpha_j\sim\frac{1}{c(0)}\sim\epsilon^{[3(D-1)/2}\sim\Gamma^{-1}\,, \tag{156b}$$

$$A_j-A_j^{(\infty)}\sim\epsilon^{(D+3)/2}\sim\Gamma^{-(D+3)/[3(D+1)]}\,, \tag{156c}$$

$$x_1-2\sim\epsilon\sim\Gamma^{-2/[3(D+1)]}\,, \tag{156d}$$

$$u-\beta u_M(\rho)\sim\epsilon^{-(D+3)/2}\sim\Gamma^{(D+3)/[3(D+1)]}\,. \tag{156e}$$

Note that in these relations the, e.g., Γ dependence of ϵ is used to express the solution entirely in terms of ϵ, with the length reduced by $a_{\rm WS}$. For the PYHS we use the hard-core diameter as the length scale and the solution is given entirely in terms of ϵ. Generalizing the 1D and 3D results,[37] we expect

$$\beta_j-2q_j\sim\epsilon^{(D+1)/2}\sim 1/g(1)\,, \tag{157a}$$

$$\alpha_j\sim 1/c(0)\sim\epsilon^{D+1}\,, \tag{157b}$$

$$A_j-2A_j^{\infty}\sim 1/g(1)\sim\epsilon^{(D+1)/2}\,, \tag{157c}$$

where $g(1)$ is the "contact" value of the PCF at $r=d$. Note that the SMSA for the OCP follows $g_{\rm max}$

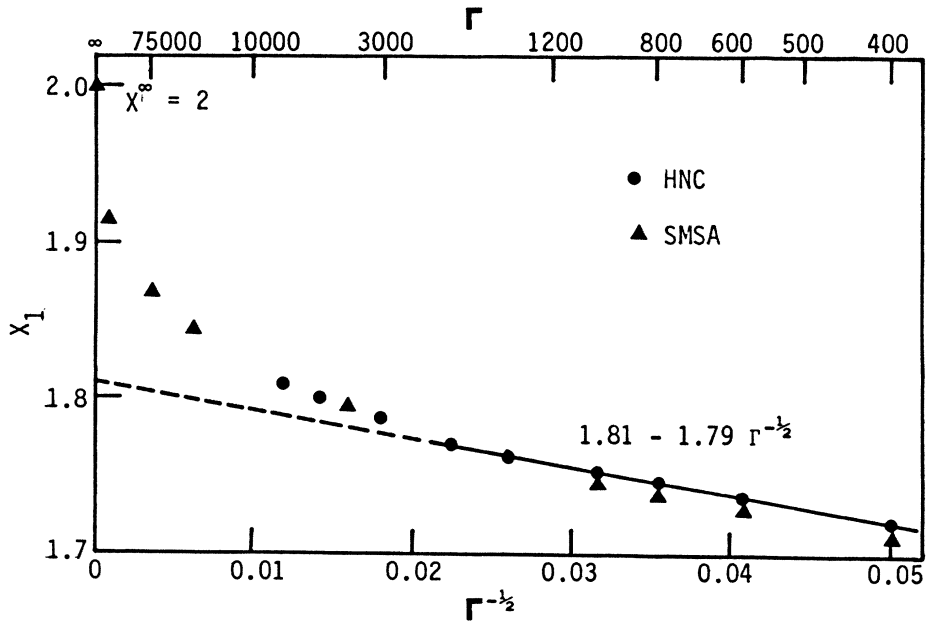

FIG. 7. Position of first peak of $g(x)$ (see text and caption of Fig. 4).

$\sim\Gamma^{1/3}\sim\epsilon^{-2}$. If the SMSA $g_{\max}$ always follows the PYHS $g(1)$ behavior $\epsilon^{-(D+1)/2}$, then $g_{\max}\sim\Gamma^{1/3}$ will hold for all D. The numerical HNC data for the OCP suggests, however, $g_{\max}\sim\Gamma^{1/2}$ for the HNC.

The nature of the AHDL behavior of the HNC theory as revealed by our analysis should be related to the bridge functions and their role in the MHNC scheme.[13,14] Note that in the "physical" fluid region, $\eta\lesssim 0.5$, it is always found that the HNC energies for repulsive potentials are higher than those obtained from computer simulations, in agreement with the short-range repulsive behavior of the bridge functions.[13] Yet, in the AHDL, the HNC potential energy provides an exact lower bound to the true potential energy of the system. This aspect of the bridge functions, and, in particular, the relation between the HNC and PY theories for hard spheres, should be clarified. It seems that the universal behavior [Eqs. (156b) and (157b)] $1/c(0)$ plays a key role in this proposed analysis. Another feature that should be clarified concerns the details of how the "Widom-theorem" behavior[38,31] of the HNC DCF's, involving an expansion in even powers near the origin, turns into an expression that contains odd powers [e.g., Eq. (38) for the OCP] when $\alpha_j=0$ (i.e., $\epsilon=0$ or $x_0=2$).

Finally, we would like to point out the important conceptual and practical implication of our results regarding the Thomas-Fermi (TF) or the more general "atom-in-box" models for the EOS of high-density matter.[39,40] Central to the TF or "atom-in-box" models is the "ion-sphere" (IS) picture in which the properties of the bulk material are approximated by those of a spherically symmetric "atom" of radius $a_{\rm WS}$, with appropriate boundary conditions for the electron distribution around the central ion that should represent the effects of the many-body correlations. The IS picture, although founded by the notion of a Wigner-Seitz lattice, is introduced, however, *ad hoc*. In the more refined density-functional theory[16] (DFT) one considers self-consistent equations for the distribution of electrons and ions around the central fixed ion. Although the ion contributions to the high-density EOS are relatively small, it is mainly the ions which determine, via the self-consistent equations, the effective potential and boundary conditions for the electronic part of the DFT problem. The IS picture is one physically suggestive way to implement the ion correlations without resort to the full self-consistency problem. What our results [and $g^{\infty}(r\le 2a_{\rm WS})=0$, in particular] mean in this context is the following:

Any DFT theory of ions and electrons, in which the ion distribution is determined by the *classical HNC* DFT, approaches, asymptotically for high densities, the corresponding TF result of an isolated (electrically neutral) sphere of radius $a_{\rm WS}$, with a uniform distribution of electrons around the central ion.

In other words, the classical HNC theory builds the ion sphere automatically in the AHDL, and there is no need to introduce it *ad hoc*. The finding that the TF theory is an exact limit of a full fledged DFT should be of help in the analysis of the boundary conditions, which represent a central issue regarding TF-like theories.[41] Our general solution of the MSA for Green's-function potentials[28] is also relevant to these studies—especially for nonspherical boundaries.[42]

ACKNOWLEDGMENTS

The author thanks H. E. DeWitt for stimulating correspondence, and L. Blum for interesting discussions and warm hospitality in Puerto Rico, where this work was completed.

APPENDIX A: RELATION OF $G_0(s)$ TO $f_{\rm HS}(t)$ FOR HARD SPHERES IN THREE DIMENSIONS

Using the OZ relation [Eq. (1)], the definitions

$$G(s)=\int_0^{\infty} r\,g(r)e^{-sr}dr\ , \tag{A1}$$

$$\hat{c}(s)=\int_0^{\infty} r\,c(r)e^{-sr}dr\ , \tag{A2}$$

and the PYHS closure, $g(r<1)=0$, $c(r>1)=0$, we obtain (with r in units of the hard-sphere diameter)

$$G(s)=\hat{c}(s)+\frac{a}{s^2}+12\eta\frac{1}{s}G(s)[\hat{c}(s)-\hat{c}(-s)]\ , \tag{A3}$$

or

$$G(s)=\frac{\hat{c}(s)+a/s^2}{1+(12\eta/s)[\hat{c}(s)-\hat{c}(-s)]}\ , \tag{A4}$$

where for the PYHS we have

$$a=1-\rho\int c(r)dr=-c(r=0)\ . \tag{A5}$$

Using the definition

$$f_{\rm HS}(r)=\lim_{\eta\to 1}[c(r)/c(0)]\ , \tag{A6}$$

and recalling that $\lim_{\eta\to 1}c(0)=\infty$, we obtain

$$G_0(s)=\lim_{\eta\to 1}G(s)=\frac{\hat{f}(s)-1/s^2}{(12/s)[\hat{f}(s)-\hat{f}(-s)]}=\frac{1}{12}\frac{s\hat{f}(s)-1/s}{\hat{f}(s)-\hat{f}(-s)}\ . \tag{A7}$$

The 3D hard-sphere Ewald function

$$f_{\rm HS}(r)=\begin{cases}1-\frac{3}{2}r+\frac{3}{2}r^3, & r\le 1\\ 0, & r\ge 1\end{cases} \tag{A8}$$

gives

$$\hat{f}_{\rm HS}(s)=-\frac{3}{s^5}e^{-s}(4+4s+s^2)+\left[\frac{1}{s^2}-\frac{3}{s^3}+\frac{12}{s^5}\right]\ , \tag{A9}$$

and when inserted into (A7) we finally obtain

$$G_0(s)=\frac{1}{12}\frac{s(s+2)}{(s+2)+(s-2)e^s}\ . \tag{A10}$$

APPENDIX B: RESIDUES OF $G_0(s)$

The poles of $G_0(s)$ are given by [with s in units of $(2a_{\rm WS})^{-1}$]

$$s_j^{\pm}=\pm i\,2q_j\ , \tag{B1}$$

where q_j are the solutions of

$$\tan q_j = q_j \ . \tag{B2}$$

Using (B1) and (B2) and the trigonometric identities

$$\cos(2q_j)=\frac{1-q_j^2}{1+q_j^2},\quad \sin(2q)_j=\frac{2q_j}{1+q_j^2}\ ,$$

we write

$$e^{s_j^{\pm}}=\frac{1-q_j^2}{1+q_j^2}\pm i\frac{2q_j}{1+q_j^2}\ . \tag{B3}$$

Denoting $L(s)=s+2$, $S(s)=s-2$, $F(s)=L(s)+S(s)e^s$, $F'(s)=1+(s-1)e^s$, the residue of $G_0(s)$ at $s=s_j$ of (B1) is given by

$$\frac{1}{12}\frac{s_j^{\pm}L(s_j^{\pm})}{F'(s_j^{\pm})}=\pm i\frac{2(1+q_j^2)}{q_j}\frac{1}{12}\ . \tag{B4}$$

The contribution to $h^{(j)}(r)$ of Eq. (71) is

$$A_j=\tfrac{1}{3}q_j\frac{1+q_j^2}{q_j^2}\ . \tag{B5}$$

When $h(r)$ is evaluated as function of $x=r/a_{\rm WS}$, then we obtain an additional factor of 2 from $d/a_{\rm WS}=2$ (for $\eta=1$), and finally

$$A_j^{\infty}=\tfrac{2}{3}q_j\frac{1+q_j^2}{q_j^2}\ . \tag{B6}$$

APPENDIX C: THE PALMER-WEEKS SOLUTION OF THE MSA FOR CHARGED HARD SPHERES (SEE SEC. VI A) (REF. 29)

The direct correlation function is given by

$$c(x)=A+6\eta M^2x+\tfrac{1}{6}\kappa^2x^2+\tfrac{1}{2}\eta(A+\kappa^2U)x^3+\frac{\eta\kappa^2x^5}{60}\ ,\quad x<1$$
$$=-\gamma/x,\quad x>1 \tag{C1}$$

where the coefficients are

$$A=-\frac{(1+2\eta)^2}{(1-\eta)^4}+\frac{Q^2}{4(1-\eta)^2}-\frac{(1+\eta)Q\kappa}{12\eta}-\frac{(5+\eta^2)\kappa^2}{60\eta}\ , \tag{C2}$$

$$U=-\frac{(1+\eta-\eta^2/5)}{12\eta}-\frac{(1-\eta)Q}{12\eta\kappa}\ , \tag{C3}$$

$$M=\frac{Q^2}{24\eta}-\frac{(1+\tfrac{1}{2}\eta)}{(1-\eta)^2}\ . \tag{C4}$$

The SMSA is obtained by finding $\eta(\Gamma)$ from the solution of $M=0$.

The Laplace transform of the PCF is (with s in units of d^{-1})

$$G(s)=sL(s)/12\eta[L(s)+S(s)e^s]\ , \tag{C5}$$

where

$$L(s)=12\eta(-Ms^2+Ps+\kappa)\ ,$$
$$S(s)=s^4+Rs^3+\tfrac{1}{2}R^2s^2+12\eta(\kappa-P)-12\eta\kappa\ , \tag{C6}$$

with

$$P=\frac{1+2\eta}{(1-\eta)^2}-\frac{Q}{2(1-\eta)}+\tfrac{1}{2}\kappa\ ,$$
$$R=\frac{6\eta}{1-\eta}-Q\ . \tag{C7}$$

The Fourier transform of the DCF is (q is units of d^{-1})

$$\rho\tilde{c}(q)=\frac{24\eta}{q^6}\left[Aq^3(\sin q-q\cos q)+6\eta M^2q^2[2q\sin q-(q^2-2)\cos q-2]+\frac{\kappa^2}{6}q[(3q^2-6)\sin q-(q^2-6)q\cos q]\right.$$
$$+\frac{\eta}{2}(A+\kappa^2U)[(4q^2-24)q\sin q-(q^4-12q^2+24)\cos q+24]$$
$$\left.+\frac{\eta\kappa^2}{60q^2}[(6q^4-20q^2+120)q\sin q-(q^6-30q^4+360q^2-720)\cos q-720]-\gamma q^4\cos q\right]\ , \tag{C8}$$

and the potential energy is given by [compare with (C3)]

$$u(\eta,\gamma)=-\frac{1}{24\eta}\left\{(1+\eta-\tfrac{1}{5}\eta^2)\kappa^2+\kappa(1+2\eta)\left[1-\left[1+\frac{2(1-\eta)^3\kappa}{(1+2\eta)^2}\right]^{1/2}\right]\right\}\equiv\frac{\kappa^2}{2}U\ . \tag{C9}$$

[1]See, e.g., J. A. Barker and D. Henderson, Rev. Mod. Phys. **58**, 587 (1976); J. P. Hansen and I. R. McDonald, *Theory of Simple Liquids* (Academic, London, 1976); *Studies in Statistical Mechanics,* edited by E. W. Montroll and J. L. Lebowitz (North-Holland, Amsterdam, 1982), Vol. VII.

[2]M. S. Wertheim, Phys. Rev. Lett. **10**, 321 (1963); J. L. Lebowitz, Phys. Rev. **133**, A895 (1964).

[3]See, e.g., D. Henderson and P. J. Leonard, in *Physical Chemistry: An Advanced Treatise* (Academic, New York, 1971), Vol. VIII B.

[4]E. Waismann and J. L. Lebowitz, J. Chem. Phys. **56**, 3093 (1976).

[5]L. Blum, Mol. Phys. **30**, 1529 (1975).

[6]L. Blum, in *Theoretical Chemistry: Advances and Perspectives* (Academic, New York, 1980), Vol. 5, p. 1.

[7]M. J. Gillan, J. Phys. C **7**, L1 (1974); A. H. Narten, L. Blum, and R. H. Fowler, J. Chem. Phys. **60**, 378 (1974).

[8]Y. Rosenfeld and N. W. Ashcroft, Phys. Rev. A **20**, 2162 (1979).

[9]See, e.g., G. Pastore, C. Napi, U. DeAngelis, and A. Forlani, Phys. Lett. **78A**, 75 (1980); D. K. Chatuverdi, G. Senatore, and M. P. Tosi, Lett. Nuovo Cimento **30**, 47 (1981).

[10]J. P. Hansen and J. B. Hayter, Mol. Phys. **46**, 651 (1982); G. Senatore and L. Blum, J. Phys. Chem. **89**, 2676 (1985).

[11]E. Waismann, Mol. Phys. **25**, 45 (1973).

[12]See, e.g., J. S. Hoye and G. Stell, Mol. Phys. **52**, 1057 (1984), for an updated list of references regarding the MSA Yukawa solution.

[13]Y. Rosenfeld and N. W. Ashcroft, Phys. Rev. A **20**, 1208 (1979).

[14]See, e.g., F. Lado, S. M. Foiles, and N. W. Ashcroft, Phys. Rev. A **28**, 2374 (1983); Y. Rosenfeld, *ibid.* **29**, 2877 (1984); J. Stat. Phys. **42**, 437 (1986); G. C. Aers and M. W. C. Dharma-Wardana, Phys. Rev. A **29**, 2734 (1984); P. Ballone, G. Pastore, and M. P. Tosi, J. Chem. Phys. **81**, 3174 (1984); C. Caccamo, G. Malesio, and L. Reatto, *ibid.* **81**, 4093 (1984); F. J. Rogers, D. A. Young, H. E. DeWitt, and M. Ross, Phys. Rev. A **28**, 2890 (1983); D. Levesque, J. J. Weis, and L. Reatto, Phys. Rev. Lett. **54**, 451 (1985); D. J. Gonsalez, M. J. Grimsom, and M. Silbert, Mol. Phys **54**, 1047 (1985); J. Wiechen, J. Phys. C **18**, L717 (1985).

[15]See, e.g., the following review articles: J. P. Hansen and M. Baus, Phys. Rep. **59**, 1 (1980); S. Ichimaru, Rev. Mod. Phys. **54**, 1017 (1982).

[16]See, e.g., M. W. C. Dharma-Wardana and F. Perrot, Phys. Rev. A **26**, 2096 (1982); J. Chihara, J. Phys. C **18**, 3103 (1985).

[17]See, e.g., the review by N. W. Ashcroft in *Studies in Statistical Mechanics,* Ref. 1.

[18]Y. Rosenfeld, J. Stat. Phys. **37**, 215 (1984).

[19]B. Barboy and W. M. Gelbart, J. Stat. Phys. **22**, 709 (1980).

[20]H. Reis, Adv. Chem. Phys. **IX**, 1 (1965); T. Boublik, Mol. Phys. **27**, 1415 (1974).

[21]H. E. DeWitt, Phys. Rev. A **14**, 1290 (1976); H. E. DeWitt and Y. Rosenfeld, Phys. Lett. **75A**, 79 (1979); A. Baram and Y. Rosenfeld, J. Phys. C **13**, L78 (1980); Y. Rosenfeld and A. Baram, J. Chem. Phys. **75**, 427 (1981).

[22](a) Y. Rosenfeld, Phys. Rev. Lett. **44**, 146 (1980); (b) J. Phys. C **13**, 3227 (1980); (c) Phys. Rev. A **24**, 2805 (1981); (d) *ibid.* **25**, 1206 (1982).

[23]Y. Rosenfeld, Phys. Rev. A **32**, 1834 (1985). Note that the mapping of the AHDL-HNC on the AHDL-SMSA was proven subject to certain conditions which are extended in the present article (Sec. V).

[24]L. Onsager, J. Phys. Chem. **43**, 189 (1939).

[25]Y. Rosenfeld, Phys. Rev. A **26**, 3622 (1982).

[26]Y. Rosenfeld and W. M. Gelbart, J. Chem. Phys. **81**, 4574 (1984).

[27]W. E. McMullen, W. M. Gelbart, and Y. Rosenfeld (unpublished).

[28]Y. Rosenfeld and L. Blum, J. Phys. Chem. **89**, 5149 (1985).

[29]R. G. Palmer and J. D. Weeks, J. Chem. Phys. **58**, 4171 (1979).

[30]J. M. Ziman, *Principles of the Theory of Solids* (Cambridge University Press, Cambridge, 1969), Sec. 2.3.

[31]K. C. Ng, J. Chem. Phys. **61**, 2680 (1974).

[32](a) The units a_{WS} are used for the poles s_j, except when noted otherwise. (b) See the remark near Eq. (151).

[33]L. Verlet, Phys. Rev. **165**, 201 (1968).

[34]See, e.g., R. R. Sari and D. Merlini, J. Stat. Phys. **14**, 91 (1976).

[35]H. Gould, R. G. Palmer, and G. Estevez, J. Stat. Phys. **21**, 55 (1979); D. MacGowan, J. Phys. C **16**, 59 (1983); also see Ref.8 above.

[36](a) F. J. Rogers and H. E. DeWitt (unpublished); (b) Y. Rosenfeld (unpublished).

[37]In 1D define $G(s)=\int g(r)e^{-sr}dr$ and get the PYHS result $G(s)=1/\{[\eta+s(1-\eta)]e^{s}-\eta\}$. The relations (157) were obtained analytically for the 1D PYHS, and from numerical study of the analytic expressions for the 3D PYHS.

[38]B. Widom, J. Chem. Phys. **39**, 2808 (1963).

[39]R. P. Feynman, N. Metropolis, and E. Teller, Phys. Rev. **75**, 1561 (1949).

[40]See, e.g., the review article by R. M. More, in *Applied Atomic Collision Physics* (Academic, New York, 1982), Vol. II.

[41]D. A. Liberman, Phys. Rev. B **20**, 4981 (1979).

[42]The solution of the AHDL-MSA variational problem for arbitrarily shaped, charged hard objects (Ref. 28 above) implies the Dirichlet boundary condition for the Thomas-Fermi problem, associated with total charge neutrality within the confined molecule. For the spherically symmetric, confined-atom, Thomas-Fermi problem, the Dirichlet and the commonly used Nuemann boundary conditions coincide.